THE JOURNAL OF PHYSICAL CHEMISTRY A

Article

Cite This: J. Phys. Chem. A 2018, 122, 4015−4022

pubs.acs.org/JPCA

OH Radical as a Probe of the Spin Polarizability in 1- and 2-Naphthol

Guadalupe Albarran,[†] Vitaly A. Rassolov,*[,‡] and Robert H. Schuler[§,∥]

[†]Instituto de Ciencias Nucleares, Universidad Nacional Autónoma de México, C.U. Ciudad de México 04510, México

[‡]Department of Chemistry and Biochemistry, University of South Carolina, Columbia, South Carolina 29208, United States

[§]Radiation Laboratory and Department of Chemistry and Biochemistry, University of Notre Dame, Notre Dame, Indiana 46556, United States

Supporting Information

ABSTRACT: The relative yields for addition of the OH radical at the various positions of 1- and 2-naphthol provide a measure of the spin polarizability in the naphthols. The observed yields show that addition occurs predominantly at the naphthol positions that are conjugated with the OH substituent. They also show that the electronic structures of the naphthols are significantly affected by a concerted interaction between the OH substituent and the unsubstituted ring and that this effect is somewhat greater when the OH substituent is adjacent to the naphthol bridge. The yields for addition at the different naphthol positions correlate with the local spin polarizabilities at reactive carbons in the naphthol. The spin polarizability may be a general property governing the reactivity of closed-shell molecules with radicals.

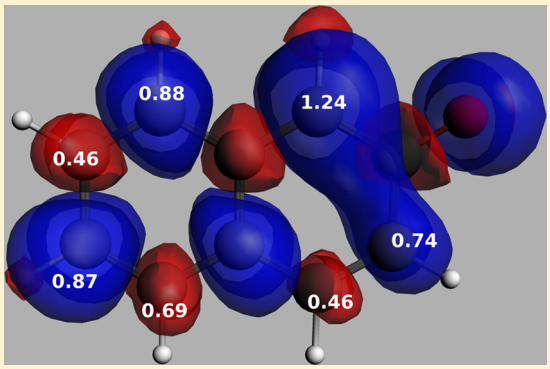

INTRODUCTION

The present study examines the distribution of products resulting from the addition of the OH radicals in aqueous solutions to 1- and 2-naphthol to provide information on the electronic structure of these naphthols. According to the conventional view, the OH radical, as a strong electrophile[1] in aqueous solution, would add preferentially at the more negatively charged sites of an aromatic. At the same time, it is well known that the relative yields of the substituted aromatics correlate reasonably well with hyperfine signals on the protons adjacent to the substitution sites measured on a corresponding radical.[2] It is possible to correlate both explanations with frontier orbital theory[3] assuming that both the radical hyperfine signal and the negative charges correlate with the amplitude of the HOMO as they do in phenol. Naphthols provide a chance to examine the adequacy of the frontier orbital picture to explain the reactivity in aromatics, as competing explanations provide different predictions of the relative yields, particularly on the sites of the unsubstituted ring in phenols. By correlating computed molecular properties with observed relative yields, we put forth a reaction mechanism based on local spin polarizability.

EXPERIMENTAL SECTION

Solutions saturated with the naphthols also containing 1 mM ferricyanide as a radical oxidant were irradiated in a ^{60}Co source and subsequently analyzed by HPLC. The methods used have been previously described.[2,4] Solutions for irradiation were prepared using reagent-grade water from a Millipore Milli-Q system. Naphthalene and the naphthols used as substrates were from Aldrich and were shown to be of high purity. Reference samples of dihydroxynaphthalenes and naphthoquinones were also from Aldrich. 1,8-Dihydroxynaphthalene, which was not available from Aldrich, was prepared by the method described by Ragot et al.[5] Its spectrum is almost identical to that of 1,5-dihydroxynaphthalene but is distinguishable because of its unusually long retention time (see below). Because this spectrum is not readily available, it is presented in Figure S1 of the Supporting Information. The naphthalene studies were conducted on a saturated concentration of ∼0.2 mM.[6] The naphthol studies were on saturated solutions.[7] All dihydroxynaphthalenes produced in the radiolysis have strong bands in the 230 nm region and weaker bands in the 300−350 nm region, which allows them to be distinguished in the chromatography. The 1,2- and 1,4-dihydroxynaphthalenes initially produced were, however, subsequently oxidized by the ferricyanide to the corresponding naphthoquinones and were identified using the strong 250 nm absorption band that is characteristic of quinones.

The solutions for irradiation were purged of dissolved air and saturated with N_2O. The N_2O served to convert the hydrated electrons to additional OH radicals. Irradiation was performed at room temperature in a ^{60}Co source at a dose rate of 8 Gy/min. Because of the low solubility of naphthalene and the naphthols, most radiolyses were carried out at doses of 0 to 120 Gy, where the products were produced at micromolar concentrations. The dose rate was determined using the Fricke

Received: November 28, 2017
Revised: April 5, 2018
Published: April 7, 2018

DOI: 10.1021/acs.jpca.7b11718
J. Phys. Chem. A 2018, 122, 4015−4022

system. Radiation chemical yields are reported here as G-values (molecules per 100 eV of absorbed energy).

Immediately after irradiation, the samples were analyzed by HPLC. Initial studies used a Waters 990 chromatography system. Subsequent studies employed an Agilent Technologies Series 1100 system. Both instruments were equipped with a diode array detector. Product separations used a Phenomenex Luna C-18 or a Thermo Scientific Hypersil BDS-CN column. Most elutions were performed with water containing 33% methanol at a flow rate of 0.45 mL/min. The eluent also contained 0.1% formic acid to maintain the products in their acidic forms. The sample volumes were 100 μL. Spectra were recorded every second to produce 3-D data files. Products were identified by the comparison of peak retention times and spectra extracted from these files with reference samples. The product concentrations were determined by using the peak areas of chromatograms extracted from the 3-D data at appropriate wavelengths. The chromatographic sensitivities were determined using the reference samples of known concentrations.

Computational studies were mostly performed on the UB3LYP/6-311+G** level of theory with the GCOSMO[8] polarizable continuum model for water as a solvent, when appropriate, as implemented in Q-Chem ver. 4.1.[9] Additional calculations were performed with the Slater-based TZP basis set using the PBEsol density functional.[10] All calculations were performed in a spin-unrestricted formalism. The spin densities at specific points in a molecule were computed using Gaussian-weighted operators with the $0.35a_0$ range parameter, as recommended by Liang and Rassolov based on the studies of organic radicals.[11]

RESULTS

Naphthalene. Previously, Kanodia et al.[6] reported that in the radiolytic oxidation of naphthalene 1- and 2- naphthol were produced in yields of 3.2 and 1.5, respectively. Because of its importance as a reference, we have critically reexamined the radiolytic oxidation of naphthalene by the methods used in the present study and have determined yields of 3.42 for the formation of 1-naphthol and 1.78 for 2-naphthol. While these yields are in reasonable agreement with the previous results, they are slightly higher and their ratio, 1.93, is somewhat lower than the ratio of 2.1 previously reported. The total, 5.20, is only slightly lower than the yield of 5.38 expected at solute concentrations of ~0.2 mM.[12,13] This total shows that the OH radical attack at the bridged positions of naphthalene is only of very minor importance.

1-Naphthol. Seven dihydroxynaphthalenes (abbreviated here as DHNs) are expected to be produced from each of the naphthols. The contour plot given in Figure 1 for 1-naphthol, obtained using the Luna C-18 column, shows, however, that only six products elute before the naphthol. The expected 1,2-DHN and 1,4-DHN are oxidized by the ferricyanide present during the radiolyses and observed as the corresponding naphthoquinones (1,2- and 1,4-NQ) at A and E. These quinones are readily recognized by their strong absorption at 250 nm that is typical of quinones. The absence of 1,2-DHN and 1,4-DHN initially produced is noted by the lack of any contribution they would be expected to make at the elution times of 39 and 25 min. Four additional products, 1,5-, 1,6-, 1,7-, and 1,3-DHN, are observed in the figure at B, C, D, and F. 1,4-NQ and 1,5-DHN are produced uniquely from 1-naphthol, and 1,2-, 1,3-, 1,6-, and 1,7-DHN are also produced

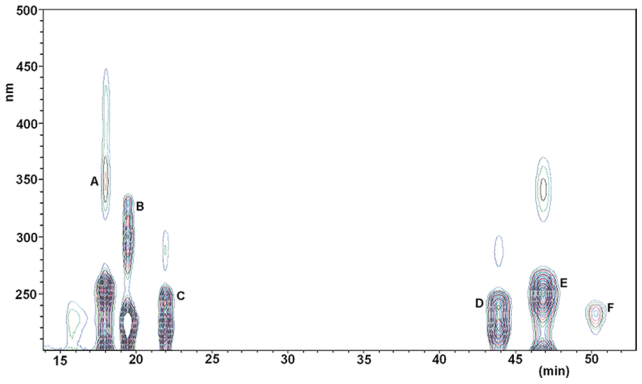

Figure 1. Contour plot for 1-naphthol irradiated to a dose of 125 Gy: (A) 1,2-NQ, (B) 1,5-DHN, (C) 1,6-DHN, (D) 1,7-DHN, (E) 1,4-NQ, and (F) 1,3-DHN. 1,8-Naphthalenediol elutes after 1-naphthol and does not appear in this figure.

from 2-naphthol. The seventh expected dihydroxynaphthalene (1,8-DHN) elutes after 1-naphthol (see below) and is not observed in Figure 1.

Figure 1 indicates that, except for the minor contribution at 15.8 min, at low doses there are no significant contributions from secondary products. At higher doses, secondary products become significant. However, they elute mostly before 1,2-NQ.

The chromatogram displayed in Figure 2, obtained using the Hypersil BDS-CN column, shows that the seventh product, 1,8-

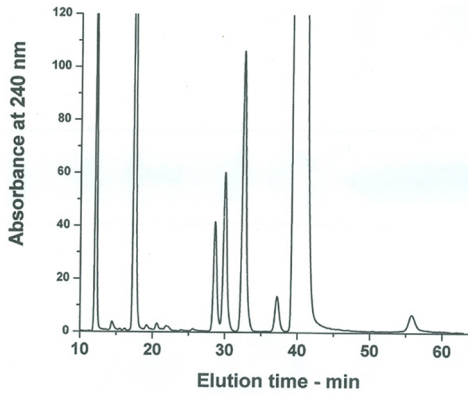

Figure 2. Chromatogram of a 1-naphthol solution irradiated to a dose of 127 Gy. The peaks are, in order of elution, ascribed to 1,2-NQ; 1,4-NQ, 1,5-DHN, 1,6-DHN, 1,7-DHN, 1,3-DHN, 1-naphthyl, and 1,8-DHN.

DHN, elutes at 56 min, i.e., well after the naphthol. Apparently, there is strong hydrogen bonding between 1,8-DHN's adjacent OH substituents that causes it to elute much more slowly than the other products.

In order to determine the initial yields ($G(P_1)_0$), the observed dose dependences ($[P_1]_D$) given in Figure 3 have been fitted by eq 1 where D is the dose and Q provides a measure of the downward curvature in the plots. (See the Appendix in ref 14 for the derivation of eq 1.)

$$[P_1]_D = G(P_1)_0 \{2(\ln (1 + QD)/Q) - D) \quad (1)$$

At low doses, the equation takes into account the increasing competition of the initial products with the naphthol and the consumption of these products in secondary reactions. The fit of the observed dose dependences to the equation was performed in ORIGIN.[15] At a dose of 30 Gy, approximately

DOI: 10.1021/acs.jpca.7b11718
J. Phys. Chem. A 2018, 122, 4015−4022

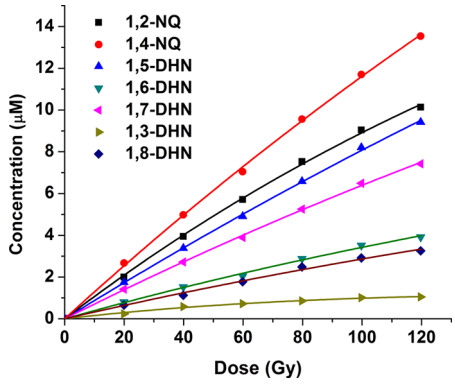

Figure 3. Dose dependencies of the products produced in the radiolysis of 1-naphthol. The solid curves represent the optimized fit of the data to eq 1.

5% of the naphthol will have been consumed, so the incremental yields of the diols at higher doses are expected to decrease as the result of competing reactions of the OH radicals with the products. The initial yields are summarized in Table 1.

Table 1. Initial Yields of the Irradiation Products of 1-Naphthol

product	position	yield
1,2-NQ	2[a]	1.08
1,3-DHN	3	0.14
1,4-NQ	4[a]	1.49
1,5-DHN	5[a]	0.99
1,6-DHN	6	0.44
1,7-DHN	7[a]	0.77
1,8-DHN	8	0.41

[a]The positions conjugated with the OH substituent.

2-Naphthol. In the case of 2-naphthol, the plot given in Figure 4 shows all seven expected products.

The 1,2-DHN produced by the OH radical addition at the 1 position of 2-naphthol is oxidized to 1,2-NQ and observed at B in the plot. The remaining expected dihydroxynaphthalenes are readily apparent in Figure 4. Of these, 2,6-, 2.7-, and 2,3-DHN are uniquely produced from 2-naphthol and observed at A, D, and G in the figure. The addition of the OH radical at 2-naphthol's 4, 5, and 8 positions results in the production of 1,6-, 1,7-, and 1,3-DHN observed at C, E, and F.

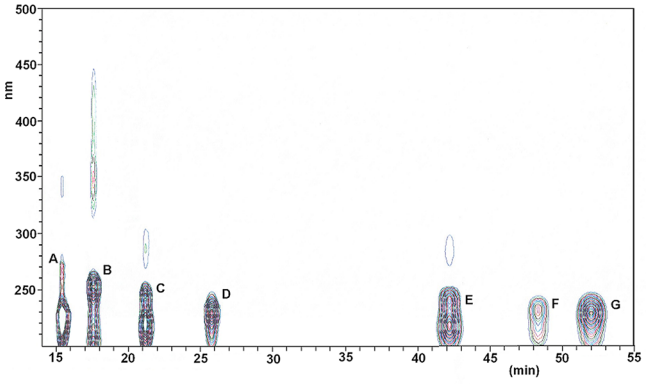

Figure 4. Contour plot for 2-naphthol irradiated to a dose of 125 Gy: (A) 2,6-DHN, (B) 1,2-NQ, (C) 1,6-DHN, (D) 2,7-DHN, (E) 1,7-DHN, (F) 1,3-DHN, and (G) 2,3-DHN.

Figure 5 displays the dose dependences of the expected products. As for 1-naphthol, the solid curves represent an optimized fit of the data to eq 1. The initial yields are summarized in Table 2.

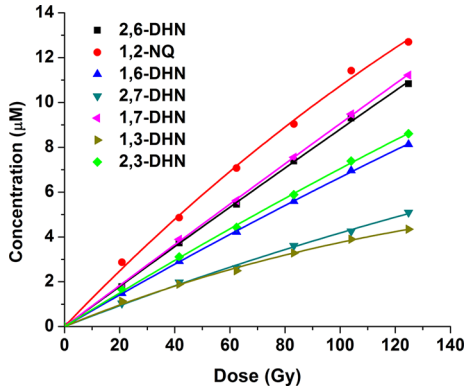

Figure 5. Dose dependencies of the products produced in the radiolysis of 2-naphthol. The solid curves represent the optimized fit of the data by eq 1.

Table 2. Initial Yields of the Irradiation Products of 2-Naphthol

product	position	yield
1,2-NQ	1[a]	1.24
2,3-DHN	3[a]	0.74
1,3-DHN	4	0.46
1,6-DHN	5	0.69
2,6-DHN	6[a]	0.87
2,7-DHN	7	0.46
1,7-DHN	8[a]	0.88

[a]The positions conjugated with the OH substituent.

COMPUTATIONAL RESULTS AND DISCUSSION

Previous studies have shown that the yields for the OH radical addition to aromatic systems correlate very well with the ESR proton hyperfine data that describe the delocalization of the unpaired spin population in the corresponding aryloxyl radicals.[2,16] For example, ESR studies show that for the phenoxyl radical the unpaired spin is located at its ortho and para positions.[17−20] Radiolytic studies, similar to those reported here, show that the OH radical addition occurs preferentially at phenol's ortho and para positions.[2,21−24] The reason for the correlation between the yields for the OH radical addition and the ESR data is not obvious, as it is highly unlikely that the naphthoxyl radicals are intermediates in the OH radical addition reaction. We envision two complementary explanations for the correlation. It is possible that the ESR data on a radical correlate with a relevant property of the closed-shell naphthol molecule, such as charge density, or a frontier orbital population. Alternatively, a reaction with the OH radical may be governed by a spin-dependent property of the aromatic system. The present study supports the latter explanation.

Figures 6 and 7 show the spin density distribution of the naphthoxyl radicals computed with the ADF suite of programs.[25] They demonstrate a correlation between the

DOI: 10.1021/acs.jpca.7b11718
J. Phys. Chem. A 2018, 122, 4015−4022

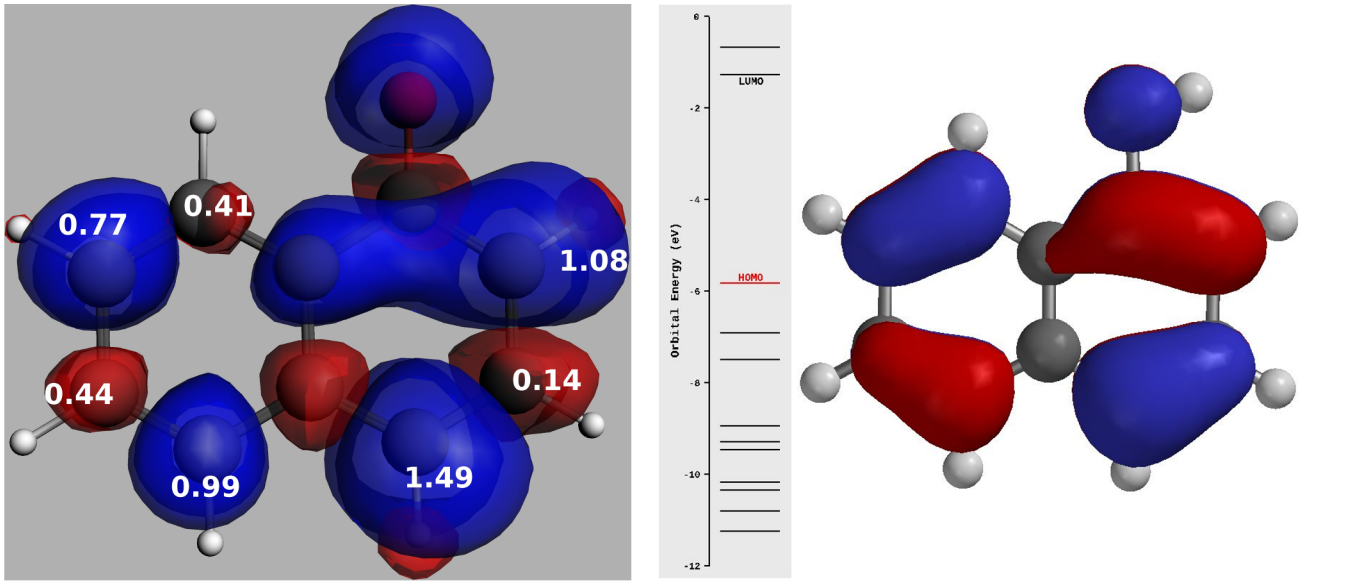

Figure 6. Spin density in the 1-naphthoxyl radical computed with ADF (left); yields for addition at the various sites of 1-naphthol are shown in white numbers; the HOMO orbital of 1-naphthol (right) is computed with Spartan.[28]

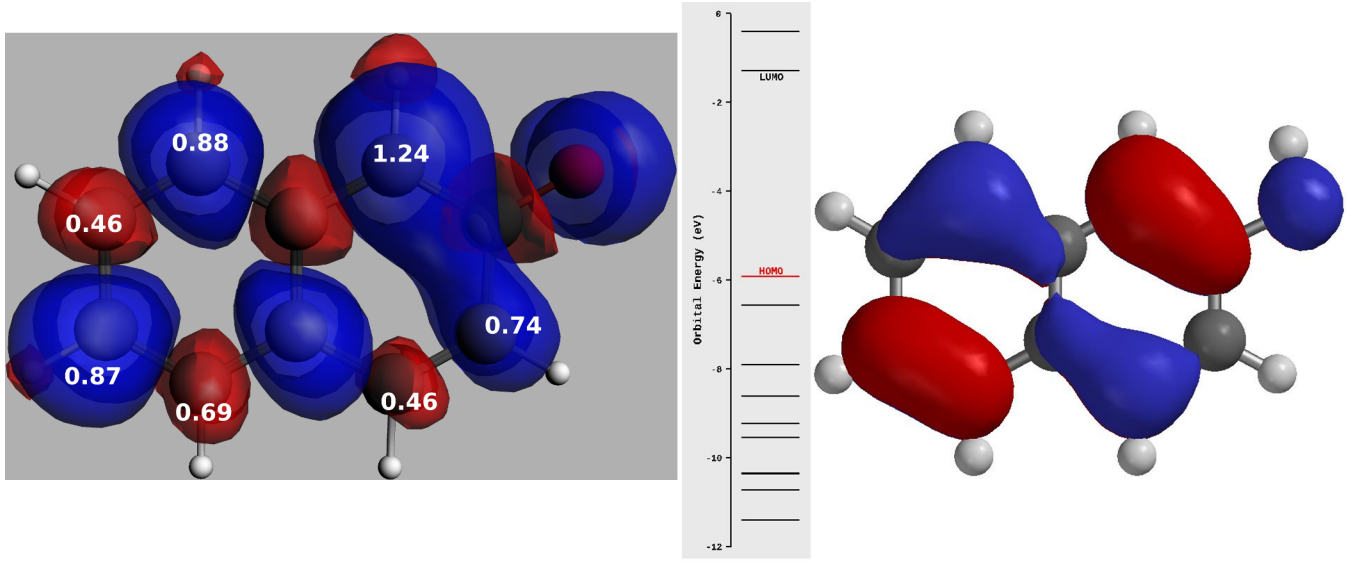

Figure 7. Spin density in the 2-naphthoxyl radical computed with ADF (left); yields for addition at the various sites of 2-naphthol are shown in white numbers; the HOMO orbital of 2-naphthol (right) is computed with Spartan.[28]

Table 3. Various Site-Dependent Properties of 1-Naphthol[a] and the 1-Naphthoxyl Radical[b,c]

site	yield	ρ(2A)	$\Delta\rho^{\sigma}$(2A)	$\Delta\rho$(2A)	ESR	$\rho^{\sigma}(H)$	$\Delta\rho^{\sigma}$ (C)	$\Delta(E)_{aq}$	$\Delta(E)_{vac}$
2	1.08	0.001242	0.000164	0.000060	*8.25*	*−0.00572*	0.012322	0.03183	0.03331
3	0.14	0.001160	0.000041	0.000109	*−1.75*	*0.00180*	0.000932	0.03029	0.02992
4	1.49	0.001202	0.000200	0.000031	*10.75*	*−0.00661*	0.013660	0.03165	0.03430
5	0.99	0.001157	0.000144	0.000009	*2.5*	*−0.00170*	0.009335	0.03503	0.03535
6	0.44	0.001164	0.000057	0.000102	*0.65*	*0.00077*	0.003593	0.03528	0.03468
7	0.77	0.001175	0.000091	0.000080	*2.50*	*−0.00177*	0.006458	0.03518	0.03545
8	0.41	0.001136	0.000108	0.000026	*0.00*	*0.00056*	0.006107	0.03450	0.03553
R		0.652	0.939	−0.762	*0.941*	*−0.949*	0.959	−0.077	0.377

[a]Columns 2−5 and 8−10. [b]Columns 6 and 7, italicized. [c]"Yield" is the experimental initial yield from the present study. "ESR" is proton hyperfine data by Murphy[27] at 10^{-4} T. "ρ" labels computed electron density, and "ρ^{σ}" labels computed spin density, all in atomic units. "$\Delta\rho$" labels the change in density between two calculations, as described in the text. The last two columns show changes in the energy of the system computed in an aqueous medium as described by the GCOSMO model[8] and labeled with an "aq" subscript, and computed energy changes in vacuum are labeled with the "vac" subscript, all in atomic units. The bottom row shows a correlation coefficient for a linear fit between the experimental yields and data in the column.

DOI: 10.1021/acs.jpca.7b11718
J. Phys. Chem. A 2018, 122, 4015−4022

Table 4. Various Site-Dependent Properties of 2-Naphthol[a] and the 2-Naphthoxyl Radical[b,c]

site	yield	ρ(2A)	$\Delta\rho^{\sigma}$(2A)	$\Delta\rho$(2A)	ESR	$\rho^{\sigma}(H)$	$\Delta\rho^{\sigma}$ (C)	$\Delta(E)_{aq}$	$\Delta(E)_{vac}$
1	1.24	0.001236	0.000231	−0.000025	*10.75*	*−0.00690*	0.016365	0.03121	0.0331
3	0.74	0.001168	0.000086	0.000085	*1.45*	*−0.00159*	0.005916	0.03760	0.0367
4	0.46	0.001129	0.000075	0.000053	*0.00*	*0.00079*	0.003476	0.03733	0.0347
5	0.69	0.001151	0.000083	0.000046	*−1.45*	*0.00121*	0.004306	0.03412	0.0334
6	0.87	0.001190	0.000109	0.000072	*5.40*	*−0.00312*	0.007690	0.03588	0.0358
7	0.46	0.001166	0.000044	0.000111	*−1.26*	*0.00126*	0.002199	0.03536	0.0340
8	0.88	0.001174	0.000167	−0.000006	*4.30*	*−0.00274*	0.010818	0.03576	0.0357
R		0.899	0.932	−0.752	*0.93*	*−0.950*	0.962	−0.690	−0.126

[a]Columns 2−5 and 8−10. [b]Columns 6 and 7, italicized. [c]"Yield" is the experimental initial yield from the present study. "ESR" is proton hyperfine data by Murphy[27] at 10^{-4} T. "ρ" labels computed electron density, and "ρ^{σ}" labels computed spin density, all in atomic units. "$\Delta\rho$" labels the change in density between two calculations, as described in the text. The last two columns show changes in the energy of the system computed in an aqueous medium as described by the GCOSMO model[8] and labeled with an "aq" subscript, and computed energy changes in vacuum are labeled with the "vac" subscript, all in atomic units. The bottom row shows a correlation coefficient for a linear fit between the experimental yields and data in the column.

unpaired spin density on carbons, with blue having the same spin as the overall S_z value of the radical and red having the opposite spin. The numbers in white show the experimental yields of the OH radical addition from the present study. Note that the spin density on the hydrogens is opposite to that of the attached carbon. The Fermi contact spin densities on the hydrogens are also computed in Q-Chem[9] using the B3LYP/6-311+G** model with Gaussian-weighted operators[26] using a 0.35 range parameter. These calculations permit us to assign the signs to the proton hyperfine data by Murphy.[27]

The experimental yields, experimental hyperfine data with our sign values, and various computed properties are shown in Tables 3 and 4. The bottom row of each table shows a linear correlation coefficient between the data and the experimental yields of the OH radical addition products. The data examines the validity of competing explanations for the reaction-yield data.

Third column "ρ(2A)" gives electron density at points 2 Å above the carbon atoms of the naphthols in the direction orthogonal to the molecular symmetry plane. The distance of 2 Å is chosen to correspond to a tail of the wave function where the electron density is small but not yet negligible so as to be overly sensitive to the numerical noise. The density at this point in space is a cumulative measure of the contribution of the most reactive orbitals, not just of the HOMO, to electron π-clouds at individual reaction sites. The HOMO alone is clearly insufficient to explain the reactivity in aromatic systems, as can be seen graphically by comparing the areas of high electron densities of the HOMO with the yield data shown in Figures 6 and 7. The ρ(2A) data correlates reasonably well with yields on 2-naphthol but does not explain the reactivity in 1-naphthol, as evident from a low correlation coefficient of 0.652.

We now explain the data in fourth column "$\Delta\rho^{\sigma}$(2A)". The reactions between the radicals and closed-shell species are often barrierless, which we confirm computationally for the OH radical addition reaction to naphthols. The chemical bond that forms upon an approach of the OH radical to a closed-shell molecule is initially due to the energetically favorable motion of the electron from a naphthol to an empty SOMO orbital on a radical. This results in a spin polarization of the closed-shell molecule by an unpaired electron of a radical. The data in the fourth column attempts to quantify such polarization on different carbons by computing the spin densities at the sites that are mirror images of those occupied by the approaching radical, which is reflected in the plane of symmetry of the naphthol. (The spin density at the site of the attack cannot be used since the OH radical has a strong direct contribution to it.) The data is obtained by placing an OH radical (at its equilibrium OH bond distance) above the chosen carbon atom along the line orthogonal to the naphthol plane of symmetry and with the O atom 2 Å away from carbon. A spin density is computed at the mirror image point to the oxygen nucleus. Seven such calculations are performed for each naphthol in the gas phase at frozen geometries, one for each reactive site. The correlation of these data with the yields is very good, comparable to that between the yields and the experimental hyperfine data on the naphthoxy radical protons shown in column "ESR". An important feature of this correlation is that the linear fit [yield(naphthol-1) = $7586.6x - 0.1113$, yield(naphthol-2) = $3939.5x + 0.3163$, $x = \Delta\rho^{\sigma}$(2A)] has relatively small intercept, in contrast to the correlation between the hyperfine data and the yields [yield(naphthol-1) = $0.09595x + 0.4461$, yield(naphthol-2) = $0.05727x + 0.6059$, x = ESR].

The spin density at the mirror points around the naphthol represents the density at the actual point of contact between the reactants only approximately. To assess this approximation, we have also computed the spin density at the carbon nucleus rather than in the mirror point. The data is shown in the eighth column labeled "$\Delta\rho^{\sigma}$(C)". Its correlation with the experimental yields is very good, the best of all data studied in this work, although the intercept of the linear fit is no longer small.

One of the main differences between the electron density and the spin polarizability is that the latter is a response property, while the former is not. To investigate a possible dependence of the yield on the spin-independent response property, we have computed the change in the total electron density at the same points as those in the "$\Delta\rho^{\sigma}$(2A)" column. The data are presented in the fifth "$\Delta\rho$(2A)" column and are computed as the difference in electron density of naphthol perturbed by an OH radical and the unperturbed density. The correlation with yields is poor and negative. The negative correlation is consistent with the importance of the electrostatic interactions for the molecular energy, which implies that the regions of high-spin polarizability are those where a molecule can maintain a nearly constant electrostatic (charge) distribution.

The calculated proton Fermi contact spin densities are presented in the seventh column "ρ^{σ}(H)". The data correlate well with the yields and with the hyperfine measurements of Murphy[27] (given in the sixth column "ESR"). This confirms

DOI: 10.1021/acs.jpca.7b11718
J. Phys. Chem. A 2018, 122, 4015−4022

that the chosen computational model is sufficiently accurate to describe the spin-dependent properties of the species involved.

The relative energies of naphthols with the OH radical at 2 Å are presented in columns 9 and 10, labeled "ΔE_{aq}" for a computation in solvent represented by a GCOSMO model[8] and labeled "ΔE_{vac}" for a computation in vacuum. Correlations with yields are very poor, probably due to the contributions of long-range electrostatic interactions to the energies of the complex at the computed geometries.

We have also attempted to correlate the observed yields with the equilibrium energies of various species. These include the final product DHNs, results of addition of the OH radical to a specific site on a naphthol "N + OH" (neutral, doublet), and ionized adducts "N + OH-e" (cations, singlet). We report solvent calculations only, although we have also computed the gas-phase energies. Most calculations are performed with the GCOSMO solvation model with the exception of the charged species in column 3, for which was semiempirical SM8 model[29] with a 6-31+G** basis was used, as implemented in Spartan.[28]

Table 5. Relative Energies of Products and Stable Intermediates in the OH Radical Addition Reaction with 1-Naphthol in kcal/mol[a]

site	yield	N1 + OH-e	N1 + OH−H	N1 + OH
2	1.08	−47.792	−2.545	−31.782
3	0.14	−32.997	−5.107	−28.901
4	1.49	−49.680	−1.706	−34.760
5	0.99	−40.376	−3.366	−33.424
6	0.44	−32.912	−3.764	−28.418
7	0.77	−37.497	−3.553	−29.560
8	0.41	−38.908	−4.686	−34.382
R		−0.902	0.963	−0.602

[a]All calculations were made with the B3LYP DFT functional with optimized geometries in water as a solvent.

Table 6. Relative Energies of Products and Stable Intermediates in the OH Radical Addition Reaction with 2-Naphthol in kcal/mol[a]

site	yield	N2 + OH-e	N2 + OH−H	N2 + OH
1	1.24	−52.371	−2.545	−36.173
3	0.74	−41.351	−4.788	−30.916
4	0.46	−37.479	−5.107	−33.156
5	0.69	−40.700	−4.788	−33.512
6	0.87	−43.909	−5.355	−29.728
7	0.46	−36.419	−6.092	−29.193
8	0.88	−46.552	−3.553	−34.076
R		−0.986	0.852	−0.583

[a]All calculations were made with the B3LYP DFT functional with optimized geometries in water as a solvent.

The energies of the OH adduct to naphthols at some sites were recently computed by Sreekanth et al.[30] in a related study and used to access the relative yields of the products. Our data, presented in fifth column "Nx + OH" (x = 1 or 2), exhibits a poor correlation between these energies and the observed yields, with correlation coefficients of linear fits of 0.6 in magnitude. Much better correlation is observed with the OH adduct products that are subsequently ionized, which are presented in 3D column "Nx + OH-e". Correlation with yields is very good, being 0.90 in magnitude for 1-naphthol and 0.99 in magnitude for 2-naphthol. A troubling aspect of this correlation is the very large energy differences between the species. The assumption that a thermal equilibrium between the computed ionized intermediates is responsible for the yields of the final products requires an effective temperature of thousands of Kelvin to explain the data. We therefore suggest that the energies of the ionized adducts are correlated to the spin polarizabilities in π-clouds, presumably because the CH bond between the hydrogen and the reactive carbon is almost orthogonal to the plane of symmetry of a naphthol, forcing a strong interaction between the hydrogen and the π-electrons. However, we cannot discount the direct influence of the energy of ionized adducts on the product yield. We should also note that the spin-unrestricted model used in the present study is known to introduce errors into spin density calculations by mixing contributions from higher-spin (quartet) states into a wave function.[31] The computed $\langle S^2 \rangle$ values are in the range of 0.75 to 0.79 for the doublet species involved in the present study, suggesting that spin contamination is not a serious problem. Nevertheless, it is likely that the accuracy of our computational model is better for the closed-shell species than for the radicals, which may explain why the best correlation with yields is obtained for the closed-shell ionized adduct products of 2-naphthol.

The energies of the final products are presented in the fourth column, labeled "Nx + OH−H". The correlation with the yields is good but positive, meaning that the most stable products have the lowest yields. It is unlikely that the energy of the final products plays a direct role in the relative yields.

We have also investigated the performance of the density functionals in the spin-polarizability calculations. We have used M06,[32] M06-2X,[32] and PBE[33] functionals, and the result for the coefficients of correlation between the observed yield and the linear fit of computed spin polarizabilities is presented in Table 7. The geometries of naphthols used in these calculations are all optimized at the B3LYP 6-311+g** level. The Minnesota M06 functional shows the best performance with the correlation coefficients the closest to unity, but the B3LYP gives qualitatively similar results.

Table 7. Correlation Coefficients for the Linear Fits between Experimental Yields and Spin Densities Computed with Various Functionals Shown in the Column Headings

	B3LYP	M06	M06-2X	PBE
N1	0.939	0.947	0.872	0.921
N2	0.932	0.947	0.901	0.861

The following reaction mechanism is consistent with our results: the first step of the reaction of the hydroxyl radical with a naphthol is irreversible, and its energetics governs the distribution of the products. The hydroxyl radical forms a bond with one of the seven reactive carbons in each naphthol creating an Nx + OH intermediate radical. It is rapidly oxidized by a ferricyanide present in the solution creating a highly acidic Nx + OH-e cationic singlet. The proton attached to the carbon bonded with an OH group is rapidly lost, yielding a product.

The first and most important step in this reaction mechanism consists of the formation of the chemical bond between the OH radical and the naphthol. The unpaired electron of the radical has to couple to the opposite-spin electron of the naphthol. The energetics of this process depends on the formation of the spin density on the naphthol, hence it is closely related, if not proportional, to the spin polarizability of the naphthol.

DOI: 10.1021/acs.jpca.7b11718
J. Phys. Chem. A 2018, 122, 4015−4022

Separately, the spin density of the naphthoxyl radicals is also related to the spin polarizabilty of the naphthol. This explains the observed correlation between the two, despite the absence of the naphthoxyl radicals in the reaction mechanism presented above.

CONCLUSIONS

We have measured the relative yields for the addition of the OH radical at the various positions of 1- and 2-naphthol. We have found that the correlation between these yields and the ESR proton hyperfine data, describing the delocalization of the unpaired spin population in the corresponding aryloxyl radicals, was less convincing than in the previous studies with the single-ring aromatic systems. The best correlation was found with the computed spin polarizability of the naphthols. The spin polarizability, or the ease with which electrons of different spin can be distorted in an electronic cloud, is related to the electron density but is not directly proportional to it. In this study, we have computed the spin polarizability approximately by perturbing a naphthol with the OH radical and computing the resulting spin density.

The correlation between the observed relative yields for the addition of the OH radical to naphthols and the spin polarizability of naphthols suggests that a conventional picture of an electrophilic attack of an aromatic system by a radical is incomplete. The reaction is likely governed by the spin polarizability of an aromatic. The interplay between the aromaticity in the rings of naphthalene with the effect of a substituent OH allows for distinguishing between the roles of spin polarizability and the electron density. The computational data on spin polarizability correlate with the experimental yields much better than with the electron density values. The conventional view of chemical bond formation also supports the notion that the spin polarizability should play a role in the initial formation of a chemical bond between a radical and a closed-shell molecule.

It is desirable to formulate and implement a direct way to compute the molecular spin polarizabilities using a perturbation theory. Correlation of the data computed this way with observed relative yields in various reactions between radicals and aromatic systems would further elucidate the role of spin polarizability in such reactions.

ASSOCIATED CONTENT

Supporting Information

The Supporting Information is available free of charge on the ACS Publications website at DOI: 10.1021/acs.jpca.7b11718.

UV spectrum of 1,8-dihydroxynaphthalene (PDF)

Absorption spectrum of 1,8-dihydroxynaphthale synthesized by the Ragot method (PDF)

AUTHOR INFORMATION

Corresponding Author

*Phone: 1-(803)-777-7811; E-mail: rassolov@mailbox.sc.edu.

ORCID

Vitaly A. Rassolov: 0000-0002-7244-8870

Notes

The authors declare no competing financial interest.

[‖]Deceased Nov 13, 2017.

ACKNOWLEDGMENTS

The work described here was supported by the Universidad Nacional Autónoma de México (grant PAPIIT-IN202916). Computational work is supported by NSF grants CHE-1048629 and OIA-1655740. V.A.R. is grateful to S. Garashchuk for the valuable comments on the manuscript.

ABBREVITATIONS

6-311+G**: Pople-style triple-ζ basis set with polarization functions on all atoms; BDS-CN: base-deactivated silica cyano (column); DHN: dihydroxynaphthalene; ESR: electron spin resonance; GCOSMO: generalized conductor-like screening model; HOMO: highest occupied molecular orbital; HPLC: high-performance liquid chromatography; NQ: naphthoquinone; PBESol: a revised-for-solids density functional of Perdew−Burke−Ernzerhof; SOMO: singly occupied molecular orbital; TZP: triple-ζ polarized (basis set); UB3LYP: spin-unrestricted model using a density functional with Becke 3-parameter exchange and Lee−Yang−Parr correlation portions

REFERENCES

(1) Neta, P.; Dorfman, L. M. Pulse Radiolysis Studies. XIII. Rate Constants for the Reaction of Hydroxyl Radicals with Aromatic Compounds in Aqueous Solutions. *Adv. Chem. Ser.* **1968**, *81*, 222−230.

(2) Albarran, G.; Schuler, R. H. Hydroxyl Radical as a Probe of the Charge Distribution in Aromatics: Phenol. *J. Phys. Chem. A* **2007**, *111*, 2507−2510.

(3) Fukui, K.; Yonezawa, T.; Shingu, H. *A Molecular*-Orbital Theory of Reactivity in Aromatic Hydrocarbons. *J. Chem. Phys.* **1952**, *20*, 722−725.

(4) Hangchun, Hu. Oxidation of Naphthols by Radiolitically Produced OH radicals. M.S. Dissertation, University of Notre Dame, Notre Dame, IN, 1991.

(5) Ragot, J. P.; Steenbeck, C.; Alcaraz, M.-L.; Taylor, R. J. K. The Synthesis of 1,8-Dihydroxynaphthalene-Derived Natural Products: Palmarumycin CP1, Palmarumycin CP2, Palmarumycin C11, CJ-12,371, Deoxypreussomerin A and Novel Analogs. *J. Chem. Soc., Perkin Trans. 1* **1999**, 1073−1082.

(6) Kanodia, S.; Madhaven, V.; Schuler, R. H. Oxidation of Naphthalene by Radiolytically Produced OH Radicals. *Radiat. Phys. Chem.* **1988**, *32*, 661−664.

(7) Yalkowsky, S. H.; He, Y.; Jain, P. *Handbook of Aqueous Solubility Data*; CRC Press: Boca Raton, FL, 2003.

(8) Klamt, A.; Schüürmann, G. COSMO: a New Approach to Dielectric Screening in Solvents with Explicit Expressions for the Screening Energy and its Gradient. *J. Chem. Soc., Perkin Trans. 2* **1993**, 799−805.

(9) Shao, Y.; Gan, Z.; Epifanovsky, E.; Gilbert, A. T. B.; Wormit, M.; Kussmann, J.; Lange, A. W.; Behn, A.; Deng, J.; Feng, X.; et al. Advances in Molecular Quantum Chemistry Contained in the Q-Chem 4 Program Package. *Mol. Phys.* **2015**, *113*, 184−215.

(10) Perdew, J. P.; Ruzsinszky, A.; Csonka, G. I.; Vydrov, O. A.; Scuseria, G. E.; Constantin, L. A.; Zhou, X.; Burke, K. Restoring the Density-Gradient Expansion for Exchange in Solids and Surfaces. *Phys. Rev. Lett.* **2008**, *100*, 136406−136406−4.

(11) Liang, L.; Rassolov, V. A. Fermi Contact Spin Density Calculations of Aromatic Radicals. *J. Phys. Chem. C* **2010**, *114*, 20648−20658.

(12) Klein, G. W.; Schuler, R. H. Oxidation of Benzene by Radiolytically Produced Hydroxyl Radicals. *Radiat. Phys. Chem.* **1978**, *11*, 167−171.

(13) Schuler, R. H.; Hartzell, A. M.; Behar, B. Track Effects in Radiation Chemistry. Concentration Dependence for the Scavenging of OH by Ferrocyanide in N_2O Saturated Aqueous Solutions. *J. Phys. Chem.* **1981**, *85*, 192−199.

DOI: 10.1021/acs.jpca.7b11718
J. Phys. Chem. A 2018, 122, 4015−4022

(14) Albarrán, G.; Schuler, R. H. Concerted Effects in the Reaction of •OH Radicals with Aromatics: Radiolytic Oxidation of Salicylic Acid. *Radiat. Phys. Chem.* **2003**, *67*, 279−285.
(15) ORIGIN PRO 8. Microcal Software: Northampton, MA, 01060 USA. 2007.
(16) Albarrán, G.; Schuler, R. H. Concerted Effects of Substituents in the Reaction of •OH Radicals with Aromatics: The Cresols. *J. Phys. Chem. A* **2005**, *109*, 9363−9370.
(17) Neta, P.; Schuler, R. H. Oxidation of Phenol to Phenoxyl Radical by Oxygen (1-) ions. *J. Am. Chem. Soc.* **1975**, *97*, 912−913.
(18) Schuler, R. H.; Buzzard, G. K. Pulse Radiolysis Experiments: Synthesis and Analysis of Composite Spectra. *Int. J. Radiat. Phys. Chem.* **1976**, *8*, 563−574.
(19) Neta, P.; Fessenden, R. W. Hydroxyl Radical Reactions with Phenols and Anilines as Studied by Electron Spin Resonance. *J. Phys. Chem.* **1974**, *78*, 523−529.
(20) Schuler, R. H. Oxidation of Ascorbate Anion by Electron Transfer to Phenoxyl Radicals. *Radiat. Res.* **1977**, *69*, 417−433.
(21) Buxton, G. V.; Langan, J. R.; Smith, J. R. L. Aromatic Hydroxylation. 8. A Radiation Chemical Study of the Oxidation of Hydroxycyclohexadienyl Radicals. *J. Phys. Chem.* **1986**, *90*, 6309−6313.
(22) Raghavan, N. V.; Steenken, S. Electrophilic Reaction of the OH Radical with Phenol. Determination of the Distribution of Isomeric Dihydroxycyclohexadienyl Radicals1. *J. Am. Chem. Soc.* **1980**, *102*, 3495−3499.
(23) Ye, M.; Schuler, R. H. Determination of Oxidation Products in Radiolysis of Halophenols with Pulse Radiolysis, HPLC and Ion Chromatography. *J. Liq. Chromatogr.* **1990**, *13*, 3369−3387.
(24) Albarran, G.; Schuler, R. H. Micellar Electrophoretic Capillary Chromatographic Analysis of the Products Produced in the Radiolytic Oxidation of Toluene and Phenol. *Radiat. Phys. Chem.* **2002**, *63*, 661−663.
(25) Baerends, E. J.; Ziegler, T.; Autschbach, J.; Bashford, D.; Bérces, A.; Bickelhaupt, F. M.; Bo, C.; Boerrigter, P. M.; Cavallo, L.; Chong, D. P.; et al. ADF2013, SCM, Theoretical Chemistry, Vrije Universiteit: Amsterdam, The Netherlands, http://www.scm.com.
(26) Rassolov, V. R.; Chipman, D. M. New operators for electronic density calculation. I. Derivations and formal analysis. *J. Chem. Phys.* **1996**, *105*, 1470−1478.
(27) Murphy, D. J. The Unpaired Electron Spin Distribution in Naphthoxyl Radicals. *J. Chem. Res.* **1980**, *S* (9), 321.
(28) Spartan'10, Wavefunction, Inc.: Irvine, CA.
(29) Marenich, A. V.; Olson, R. M.; Kelly, C. P.; Cramer, C. J.; Truhlar, D. G. Self-Consistent Reaction Field Model for Aqueous and Nonaqueous Solutions Based on Accurate Polarized Partial Charges. *J. Chem. Theory Comput.* **2007**, *3*, 2011−2033.
(30) Sreekanth, R.; Prasanthkumar, K. P.; Sunil Paul, M. M.; Aravind, U. K.; Aravindakumar, C. T. Oxidation Reactions of 1- and 2-Naphthols: an Experimental and Theoretical Study. *J. Phys. Chem. A* **2013**, *117*, 11261−11270.
(31) Chipman, D. M. The Spin Polarization Model for Hyperfine Coupling Constants. *Theor. Chim. Acta.* **1992**, *82*, 93−115.
(32) Zhao, Y.; Truhlar, D. G. The M06 Suite of Density Functionals for Main Group Thermochemistry, Thermochemical Kinetics, Noncovalent Interactions, Excited States, and Transition Elements: Two New Functionals and Systematic Testing of Four M06-Class Functionals and 12 other Functionals. *Theor. Chem. Acc.* **2008**, *120*, 215−241.
(33) Perdew, J. P.; Burke, K.; Ernzerhof, M. Generalized Gradient Approximation Made Simple. *Phys. Rev. Lett.* **1996**, *77*, 3865−3868.

DOI: 10.1021/acs.jpca.7b11718
J. Phys. Chem. A 2018, 122, 4015−4022